Yb-to-Eu Cooperative Sensitization Upconversion in a Multifunctional Molecular Nonanuclear Lanthanide Cluster in Solution

Sai P.K Panguluri, Elsa Jourdain, Papri Chakraborty, Svetlana Klyatskaya, Manfred M Kappes, Aline M Nonat, Loïc J Charbonnière, Mario Ruben

Yb to Eu cooperative sensitization upconversion in a multifunctional molecular nonanuclear lanthanide cluster in solution

Sai P.K. Panguluri,[a] Elsa Jourdain,[b] Papri Chakraborty,[d] Svetlana Klyatskaya,[d] Manfred M. Kappes,[d] Aline M. Nonat,[b]* Loïc J. Charbonnière,[b]* Mario Ruben,[a,c,d]*

[a] Institute of Quantum Materials and Technologies (IQMT), Karlsruhe Institute of Technology, Kaiserstraße 12, 76311 Karlsruhe, Germany

[b] Equipe de Synthèse pour l'Analyse (SynPA), Institut Pluridisciplinaire Hubert Curien (IPHC), UMR 7178, CNRS/Université de Strasbourg, ECPM, France

[c] Centre Européen de Sciences Quantiques, Institut de Science et d'Ingénierie Supramoléculaires (ISIS, UMR 7006), CNRS-Université de Strasbourg, 8 allée Gaspard Monge BP 70028 67083 Strasbourg Cedex France, France

[d] Institute of Nanotechnology, Karlsruhe Institute of Technology (KIT), Kaiserstraße 12, 76311 Karlsruhe, Germany

KEYWORDS: Lanthanides, Upconversion, Clusters, Single molecular magnet.

ABSTRACT: Lanthanide metal clusters excel in combining molecular and material chemistry properties. Here, we report an efficient cooperative sensitization UC phenomenon of a Eu^{3+}/Yb^{3+} nonanuclear lanthanide cluster in CD_3OD. The synthesis and characterization of the heteronuclear cluster in solid state and solution is described together with the UC phenomenon showing Eu^{3+} luminescence in the visible region upon 980 nm NIR excitation of Yb^{3+} at concentrations as low as 100 nM. Alongside being the Eu/Yb cluster to display UC (with a quantum yield value of 4.88 x 10^{-8} upon 1.13 W cm^{-2} excitation at 980 nm), the cluster exhibits downshifted light emission of Yb^{3+} in the NIR region upon 578 nm visible excitation of Eu^{3+}, which is ascribed to sensitization pathways for Yb through the $^5D_0$ energy levels of Eu^{3+}. Additionally, a faint emission is also observed at *ca* 500 nm upon 980 nm excitation, originating from cooperative luminescence of Yb^{3+}. The $[Eu_8Yb(BA)_{16}(OH)_{10}]Cl$ cluster (BA = benzoylacetonate) is also a field-induced single molecular magnet (SMM) under 4K with a modest U_{eff}/k_B = 8.48 K, thereby joining the coveted list of Yb-SMMs and emerging as a prototype system for next-generation devices, combining luminescence with single molecular magnetism in a molecular cluster.

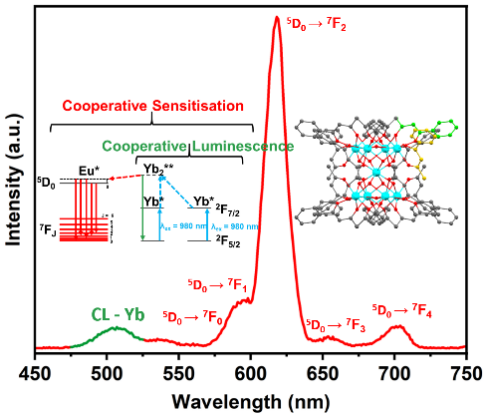

Introduction:

The unique electronic properties of lanthanides have enabled them to play a crucial role in developing modern technologies. They are routinely employed in LEDs,[1] medical X-ray computed tomography imaging,[2] anti-counterfeiting pigments,[3] and strong permanent magnets for diverse applications like MRI scanners and magnetic levitation trains. Additionally, their outstanding optical properties, intricate energy diagrams,[5] and extended lifetimes,[6] drive the development of luminescent tags for bio-analysis[7] and microscopy.[8,9,10]

In particular, the development of materials[11-14] and molecules[15-17] capable of luminescence upconversion (UC) is booming. UC is the process in which the energy from multiple incoming photons absorbed by a material or a molecule is reemitted in the form of a single photon of higher energy than the incident light, resulting in an anti-Stokes process. The UC phenomena can be categorized under two broad divisions based on the suggestive mechanisms, a classification that has evolved since the pioneering theoretical work of M. Göppert-Mayer and N. Bloembergen in the 1930s-60s.[18a,b] The non-linear processes, such as two-photon absorption excitation and second harmonic generation (SHG),[18c] fall into one division. These processes are predicated as weakly efficient as they are based on virtual excited states. The second category of UC processes involves the sequential absorption of individual photons, resulting in improved efficiency **(Fig 1.)**. These mechanisms are excited state absorption (ESA), energy transfer UC (ETU), cooperative sensitization (CS), and cooperative luminescence (CL). ESA **(Fig 1a.)** involves the absorption of a photon leading to an intermediate excited state, subsequently absorbing a second photon to reach the emitting UC luminescent level.[19] In the ETU mechanism reported by François Auzel **(Fig 1b.)**,[20,21] the second photon absorption occurs on another ion in the molecule, and an energy transfer occurs between the two ions to feed the emitting upper excited state. CS **(Fig 1c.)** is an interplay between three atoms. Two donor atoms transfer their energy to the third one,

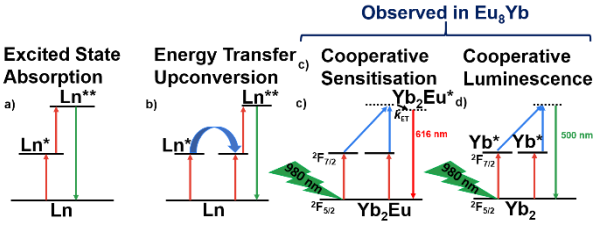

Figure 1. Upconversion mechanisms. a) Excited state absorption. b) Energy transfer upconversion. c) Cooperative sensitization of Eu in Yb_2Eu. d) Cooperative luminescence from Yb_2.

which emits light.[22,23] This mechanism is the most frequent in molecular upconverters based on the Tb^{III}/Yb^{III} pair where the $^5D_4$ excited state of Tb^{3+} around 20 600 cm^{-1} is populated through the Yb^{3+} $^2F_{5/2}$ excited state at approximately 10 200 cm^{-1}.[24,25,26,27] Finally, cooperative luminescence (CL) is achieved when the interaction of pairs of lower-energy excited states cooperatively interact to produce the emission of photons at a higher excited state **(Fig 1d.)**. This phenomenon has been reported on solid-state materials [28,29] and more recently using homonuclear Yb^{3+} clusters[26,30] or dimers in solution.[31a] These cooperative processes are treated by two operators transitions between pair levels; they are generally less efficient than ESA or ETU. [31b]

A considerable amount of research has been done on UC, and most of it is based on lanthanide-based solid materials[19,20,21,22] or nanoparticles.[32,33,34,35] The growing interest in UC materials for biological applications has led to a focus on scaling down UC to the molecular level. This approach aims to enhance solubility, reduce toxicity, improve stability, and create environmentally friendly and reproducible molecular assemblies. The study of molecular-scale UC in solution has gained attention over the past decade, with coordination chemistry playing a central role.[36,37] To observe UC, three prerequisites must be met. Firstly, the elements used for UC emission must have a ladder-like energy level diagram to climb to the higher excited state. This can be achieved by using a single element (*e.g.,* ESA with Er^{3+} [38,39,40]) or by using a pair or combination of elements – donors and acceptors – such as Yb^{III}/Er^{III},[41,42] Yb^{III}/Tb^{III},[24,25,26,27] Cr^{III}/Er^{III} [43,44] or Ru^{III}/Yb^{III} [45] for ETU and CS. The only exception is the cooperative luminescence, which can be observed from the single Yb^{3+} $^2F_{5/2}$ excited state of Yb^{3+}.[26,46] In all cases, the intermediate excited states must possess long lifetimes to guarantee an uninterrupted process leading to the population of the upper state before its return to the ground state through decay. The spatial proximity of energy donors and acceptors[47] is another key to exhibiting energy transfer and, thus, UC. In the last decade, molecular upconversion in solution has been achieved by reducing the de-excitation pathways of Ln(III) complexes, selecting appropriate donor-acceptor pairs, and arranging them spatially. This accomplishment was made possible by designing discrete heteropolynuclear coordination complexes[24,25,39,44,48] and molecular clusters.[26,30,31]

More specifically, the authors had previously reported the synthesis of homo-and hetero-nonanuclear Ln^{III} complexes with β-diketonate ligands and, more precisely, acetylacetonate ligands and their deuterated analogs.[26,30] They demonstrated that the obtained clusters are stable in organic solvents such as methanol. Upconversion studies of the homonuclear Yb_9 cluster $[Yb_9(acac)_{16}(OD)_{10}](OD)$ in CD_3OD revealed the emergence of an emission band at 503 nm when irradiated with 980 nm light, marking the occurrence of molecular CL upconversion in a solution for the first time. Additionally, hetero-nonanuclear complexes containing both Tb^{III} and Yb^{II}, such as $[Tb_xYb_{9-x}(acac)_{16}(OD)_{10}](OD)$, demonstrated CS upconversion, wherein the energy transfer originated from two excited state of Yb^{III} to sensitize Tb^{III}. The deuteration of the ligands as well as the optimization of the donor (Yb^{III}) : acceptor (Tb^{III}) ratio, allowed for the generation of a highly intense upconversion signal with a UC quantum yield of ϕ_{UC} = 2.8 x 10^{-6} upon excitation at 980 nm (CD_3OD, P = 2.86 W. cm^{-2}).[26,30] Based on these previous studies, we turned towards a mixed Eu^{III}: Yb^{III} nonanuclear $[Eu_8Yb(BA)_{16}OH_{10}]Cl$ cluster with benzoylacetonate (BA) ligands **(Figure 2)**. Here, we present the synthesis of the cluster and its characterization in the solid state and, in solution, its magnetic properties as a Yb-SMM as well as its luminescent properties in the visible (Eu^{III}) and in the NIR (Yb^{III}) upon excitation in the BA antenna. Last but not least, direct CS upconversion of Eu^{III} is also achieved while irradiating Yb at 980 nm. Although indirect photosensitization was reported from Tb to Eu,[49a] UC has only been reported once for a Eu^{III}: Yb^{III} pair in a molecular complex and in solution through an excited multimer process.[49b] Isostructural clusters with other lanthanides (Eu, Gd, Tb, Ho, Yb, Dy) and Y have also been synthesized and examined for comparison.

Results and discussion

Synthesis and crystal structure. A series of five homonuclear nonanuclear clusters of general composition $[Ln_9(BA)_{16}(OH)_{10}]Cl$ (Ln = Eu, Gd, Tb, Ho, Yb) and three heteronuclear clusters of respective formulae $[Eu_8Yb(BA)_{16}(OH)_{10}]Cl$, $[Dy_8Yb(BA)_{16}(OH)_{10}]Cl$ and $[Y_8Dy(BA)_{16}(OH)_{10}]Cl$ (BA = benzoylacetonate) were synthesized in 59-70% yields using modified procedures from existing literature **(Figure 2a)**.[49c] The synthetic methodology, together with their crystal structures as determined by X-ray crystallography, are presented in **Figure 2**. Clusters have been characterized by XRD, ESI-TOF mass spectrometry, and elemental analysis (see SI).

The nonanuclear clusters crystalize in a high cubic symmetry packing (a = b = c = 33.6739(6) Å, $\alpha = \beta = \gamma$ = 90°, V = 38183.9 $Å^3$, Pn3n (222)). This closed-packed arrangement results in hexagonal channels (voids) along the body diagonal directions inside the massive unit cell (SI. 2.1 Figure 11.). The diameter of the channel changes as it runs, with a minimum diameter of approximately 7 Å, not including the van der Waals volume. The channel is spacious enough for solvent molecules and anions (Cl^-) to situate themselves. Within the lattice, the channels stretch along the four-body diagonal directions of the unit cell, causing significant disorder among smaller components. Even at 120 K, X-ray analysis cannot resolve this disorder. The solid-state structure of the Ln_9 complexes can be

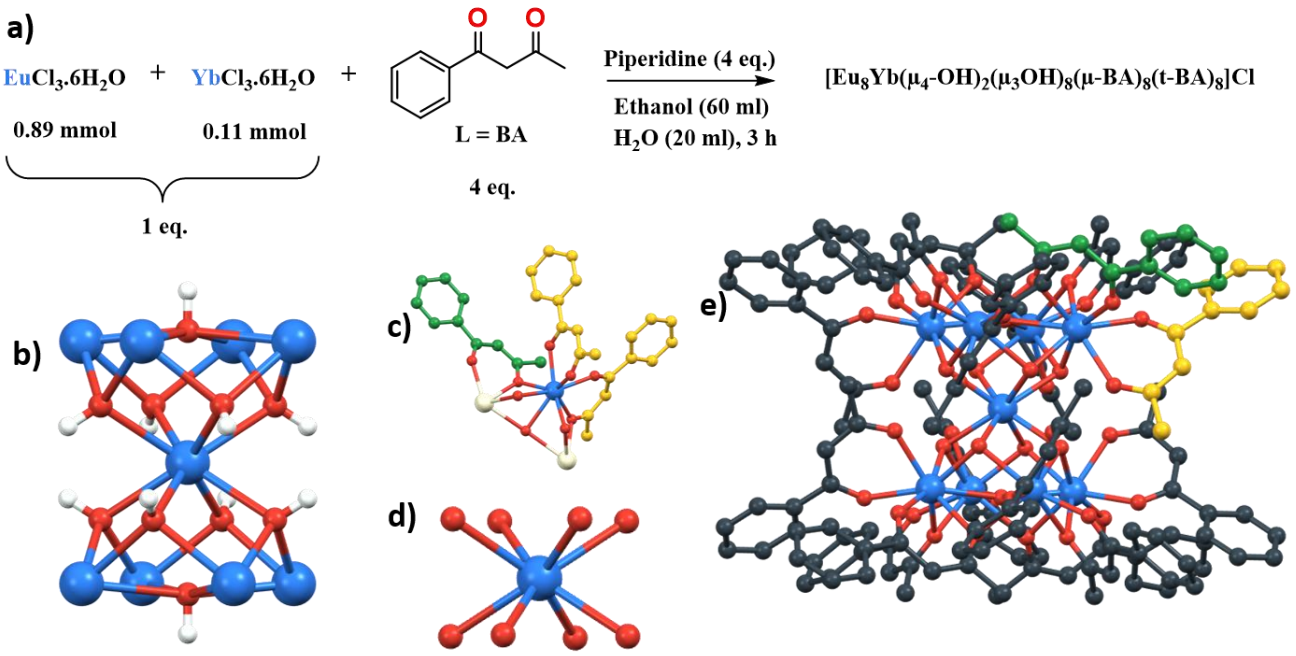

Figure 2. a) Synthetic protocol for preparing the nonanuclear Eu_8Yb complex. B) Single crystal X-ray structure of $[Eu_8Yb(BA)_{16}(OH)_{10}]Cl$ showcasing the arrangement of the nine Ln (blue) and ten hydroxyl groups (O in red and H in white). C) $Ln_{Peripheral}$ coordination sphere: endo ligands (yellow), exo ligands (green), neighboring metal ions(white), oxygens (red). D) $Ln_{Central}$ coordination sphere.

viewed as two pentanuclear square pyramids sharing the apical Ln atom, with a torsion angle of approximately 45° between the two pyramids, resulting in square anti-prismatic geometry at the central Ln **(Figure 2b)**. The eight triangular faces of the pyramids are capped by μ_3-OH groups linked to the three Ln at the edges of the triangles, while μ_4-OH bonds connect the four Ln atoms of the two square faces. All Ln atoms except the central one are linked to three β-diketonate ligands through two coordination modes (*t*-BA in yellow and μ-BA in green, **Figure 2c and 2e**). The peripheral Ln ions are coordinated by 16 bidentate BA ligands. Eight of them (shown in yellow, Figure 3e) present an *endo* environment with a bidentate coordination mode to a single metal center (*t*-BA), while the eight others (shown in green, **Figure 2e**) are placed in an *exo* environment and coordinate two metal centers in a bridging mode (μ-BA), while being bidentate coordinated to one of the two metals. The coordination sphere of Ln atoms (CN = 8) is completed by hydroxyl ligands: two μ_3-OH hydroxy ligands in the triangular face and μ_4-OH ligands in the square face. The central lanthanide is octacoordinated with eight μ_3-OH hydroxy ligands **(Figure 2b)**. In the following discussion, these two distinct coordination environments will be referred to as $Ln_{peripheral}$ and$Ln_{central}$, respectively. Previous studies have shown that such distinct coordination environments can be used to promote site selectivity for heteronuclear lanthanide clusters, with a tendency for the largest ion to occupy the central position.[50] In order to very if site selectivity was also present in the BA-clusters, a set of eight homo- and heterometallic nonanuclear clusters was synthesized and crystallized (SI. 2.1. Table 1). Continuous shape measures (CShMs) were conducted on X-ray crystallographic data within series, revealing that the $Ln_{central}$ site exhibits a nearly perfect square antiprismatic geometry with D_{4d} symmetry, while the $Ln_{peripheral}$ site is a biaugmented trigonal prism with C_{2v} symmetry. In addition, the "coordination site cavity" (also called "pocket size") for the two different environments was determined by averaging the Ln-O bond lengths (SI Figures 1-10) for each site.[51] The study demonstrated that the central pocket size is the largest (SI. 2.1. Table 1). However, refining the occupancy of each lanthanide site as a superposition of *x* Ln_1 and *(1-x)* Ln_2 did not reveal notable site preferences in the cases of

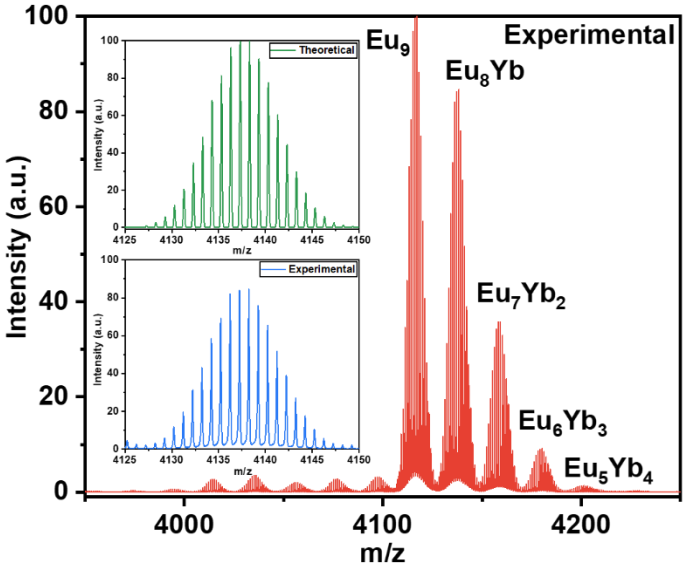

Figure 3. ESI mass spectrum in positive ion mode of the $[Eu_8Yb(BA)_{16}(OH)_{10}]^+$ complex sprayed from a methanol solution. Insets show

Eu/Yb, Dy/Yb, and Y/Dy due to the minimal difference in their ionic radii. The refined values were: $Ln_{Central}$: 96 ± 5% Eu, 4 ± 5% Yb; $Ln_{Peripheral}$: 92 ± 4% Eu, 8 ± 4% Yb.

SEM-EDS analysis gave an atomic composition of 81.3% Eu, 9.6% Yb, and 9.2% Cl, in good agreement with the predicted values of 80% Eu, 10% Yb, and 10% Cl (SI. 2.2. Fig. 13). The phase purity was also confirmed by measuring the PXRD of fresh crystals taken from the mother liquor (SI. 2.3. Fig. 14). The crystals that are dried and taken from the vacuum lost the order (SI. 2.3. Fig 15). However, a thermal stability study by thermogravimetric analysis (SI. 2.4 Fig 16) confirmed that the compounds remain stable up to 150°C and a weight loss of approximately 5% was measured in the temperature range 0 - 100°C, which corresponds to the loss of lattice solvent (three EtOH and four H_2O molecules), in perfect agreement with PXRD studies. At temperatures above 210°C, decomposition of the cluster is observed.

To confirm for the homogeneity of the bulk, SEM-EDS analysis was performed on both crystals and powder samples of Eu_8Yb complex at five different sites, giving an atomic composition of 88.6% of Eu and 11.4% of Yb, in good agreement with the 88.9% of Eu and 11.1% of Yb, introduced in the synthesis (SI. 2.2. Fig. 12.). The atomic composition in C and H was also verified by elemental analysis (SI. 2.5. Table 2).

ESI-TOF Mass Analysis Finally, the composition of the cluster in solution was analyzed by electrospray ionization mass spectrometry (ESI-MS). The resulting spectrum **(Figure 3.)** showed primary peaks at *m/z* 4116, 4137, and 4158, corresponding to the monocharged Eu_9, Eu_8Yb, and Eu_7Yb_2 complexes, respectively. The other peaks on the higher *m/z* side with intensity <10% of the most abundant Eu_9 peak are due to complexes with higher Yb replacing Eu in the metal core (Eu_6Yb_3, Eu_5Yb_4). Full range ESI MS spectrum is presented in the supporting information (SI. 2.6. Fig.17.). The relative integrals of the isotopic patterns were used to calculate the proportion ($\boldsymbol{P_i}$) of the Ln^1 and Ln^2 species at a mole fraction $\boldsymbol{x}$ of Ln^1. Experimental values ($P_{0,\mathrm{exp}} = 0.41$ for [Eu_9]; $P_{1,\mathrm{exp}} = 0.37$ for [$YbEu_8$]; $P_{2,\mathrm{exp}} = 0.17$ for [Yb_2Eu_7]; $P_{3,\mathrm{exp}} = 0.05$ for [Yb_3Eu_6] and $P_{4,\mathrm{exp}} = 0.008$) demonstrate an overall good agreement with the perfect statistic distribution as obtained by Equation (2), under the hypothesis that all coordination sites in the clusters are chemically equivalent and all Ln(III) clusters have similar ionization abilities:

$$\boldsymbol{P_i} = \frac{\boldsymbol{n!}}{\boldsymbol{i!(n-1)!}} * \boldsymbol{x^i(1-x)^{n-i}} \quad (2)$$

where n represents the total number of sites, *i.e.* 9 in a nonanuclear complex; $\boldsymbol{i}$ represents the number of Ln^1 ions (here Yb); $\boldsymbol{x} = 1/9$; $P_{0,\mathrm{th}} = 0.346$ for [Eu_9]; $P_{1,\mathrm{th}} = 0.389$ for [$YbEu_8$]; $P_{2,\mathrm{th}} = 0.195$ for [Yb_2Eu_7]; $P_{3,\mathrm{th}} = 0.057$ for [Yb_3Eu_6] and $P_{4,\mathrm{th}} = 0.011$).

Complexes with a higher molar fraction of Yb have a probability lower than 1%. This analysis also shows that for a Yb:Eu stoichiometric ratio of 1:8, complexes containing at least two Yb atoms represent more than 22% of all possible nonanuclear complexes formed, which is favorable to the observation of molecular upconversion with a CS mechanism (see below).

Magnetic Measurements. Trivalent lanthanide ions possess a strong spin-orbit coupling, resulting in their highly anisotropic nature. This feature has led to the emergence of various coordination compounds of Ln(III) exhibiting SMM behavior.[52] The increasing popularity of single molecular magnetism in recent years is due to the potential use of SMMs in various quantum technological fields. The vast majority of Ln^{3+} complexes featuring photoluminescence and SMM behavior are based on Dy^{3+}, closely followed by Yb^{3+} complexes. SMMs based on Yb would require a strong axial magnetic anisotropy and, with appropriate system designs, can reach energy barriers of magnetization reversal as high as 45 cm^{-1}.[53] Furthermore, Yb complexes emitting in the Near Infrared (NIR) region are particularly intriguing due to the potential for combining magnetic properties with luminescence, offering prospects for advanced information storage and quantum computing applications.[54] To the best of our knowledge, no compounds exhibiting both Upconversion (UC) luminescence and field-induced SMM behavior have ever been reported. In this study, we analyzed the dc magnetic behavior of Eu_8Yb (using a weighted average of all the clusters as MW found in the Mass spectrum (SI. 2.7.)) under a 1000 Oe magnetic field in the temperature range of 2-300 K. **(Figure 4a)** shows the corresponding $\chi_m T$ *vs.* T dependencies. As the temperature decreases from 300 K to 2K, there is a consistent decrease in $\chi_m T$ for all nonisotropic lanthanide-containing complexes. This can be attributed to the depopulation of the m_j levels split by the crystal field and the weak antiferromagnetic intermolecular interactions between Ln^{3+} ions. The dependencies of $\chi_m T$ *vs.* T, especially the low value at low T, indicate the incorporated Eu^{3+} ion's absence of thermally populated excited states and highlight their decisive effect on the dc magnetic behavior. Therefore, the sole contributor of $\chi_m T$ at 2 K is Yb^{3+}, which explains the very low value, as Eu^{3+} has no contribution at such low temperatures. In contrast, at 300 K, the $\chi_m T$ value is 17.47 cm^3 K mol^{-1}, and the calculated value is eight times 1.7 (Eu^{3+}) and 2.57 (Yb^{3+}) = 16.14 cm^3 K mol^{-1} for nine non-interacting ions. The small discrepancy is within the acceptable range of a 10% error. Since Yb^{3+} has a prolate electron density and, therefore, is anisotropic, we investigated the magnetization dynamics by ac susceptibility measurements on the same sample under an applied dc field of 1750 Oe, in order to establish whether the properties of the single molecule magnets (SMMs) are exhibited (**Figure 4b, d**). The slow relaxation magnetic behavior, which may originate from the significant separation between the ground and the first excited state, was investigated. No out-of-phase signal was observed at zero dc field, likely due to quantum tunneling of the magnetization (QTM), which is enabled by the mixture of the M_J levels in the ground state. However, a clear out-of-phase signal was observed upon applying a small dc field. Under a static dc field of 1750 Oe, the signal of the ac magnetic susceptibility was optimized in the frequency range of 1 to 1500 Hz, where an out-of-phase signal was

observed up to 5.6 K (**Figure 4d**). These data were fit to a generalized Debye model from which a distribution (α) of relaxation times (τ) can be extracted. Further insights into the magnetic relaxation processes of the complex were achieved by evaluating the ln(τ^{-1}) vs. T plot (**Figure 4c**). Considerable deviation from the linear course of the dependencies evidences the occurrence of the relaxation mechanisms additional or different from the Orbach one. Hence, the fit by other mechanisms and/or their sums were performed.

$$\tau^{-1} = \underbrace{\tau_0^{-1} \exp(-U_{eff}/k_BT)}_{\text{Orbach}} + \underbrace{CT^m}_{\text{Raman}} + \underbrace{\tau_{QTM}^{-1}}_{\text{QTM}} \qquad (3)$$

The fittings by the sets of mechanisms other than the Raman fit were unsatisfactory and/or led to overparameterization. As a consequence, we approximated the relaxation data in the entire temperature range by the Raman relaxation mechanism ($\tau_{Raman}^{-1} = C_{Raman} \cdot T^{m\text{-}Raman}$). We also fitted the data with an additional Orbach contribution owing to the linearity of the data points (deviation from exponential behavior) at temperatures above 3K to determine the effective energy barrier and the relaxation time. The resulting best-fit parameters are $\tau_0 = 4.4 \times 10^{-6}$ s, $U_{eff}/k_B = 8.48$ K, C = 718.46 s^{-1} $K^{-2.27}$, m = 2.27. These parameters indicate that the $YbEu_8$ cluster exhibits SMM behavior, characterized by a relatively short relaxation time and a moderate energy barrier, especially when compared to other SMMs based on Yb^{III} reported in the literature.[55] This is, to the best of our knowledge, the first example of a Yb^{III}-based SMM that also possesses upconversion properties (as illustrated below). Throughout the temperature range (2 – 4 K), the exponentially increasing τ^{-1} values plotted on a logarithmic scale confirm the presence of a Raman relaxation process. Finally, at high temperatures, deviation from this exponential behavior might suggest the onset of an Orbach relaxation mechanism, which has been observed in a limited number of Yb^{III}-based complexes. [53,56,57] The combination of luminescence(see below) and magnetic properties has also attracted interest due to the possible correlation between the electronic structure of complexes extracted from optical properties and the effective energy barriers determined by dynamic magnetic measurements.[58] Furthermore, beyond just understanding the SMM behavior, Light can be used as a non-invasive trigger to manipulate the spin state of a system, while optical measurements can act as probes to study the

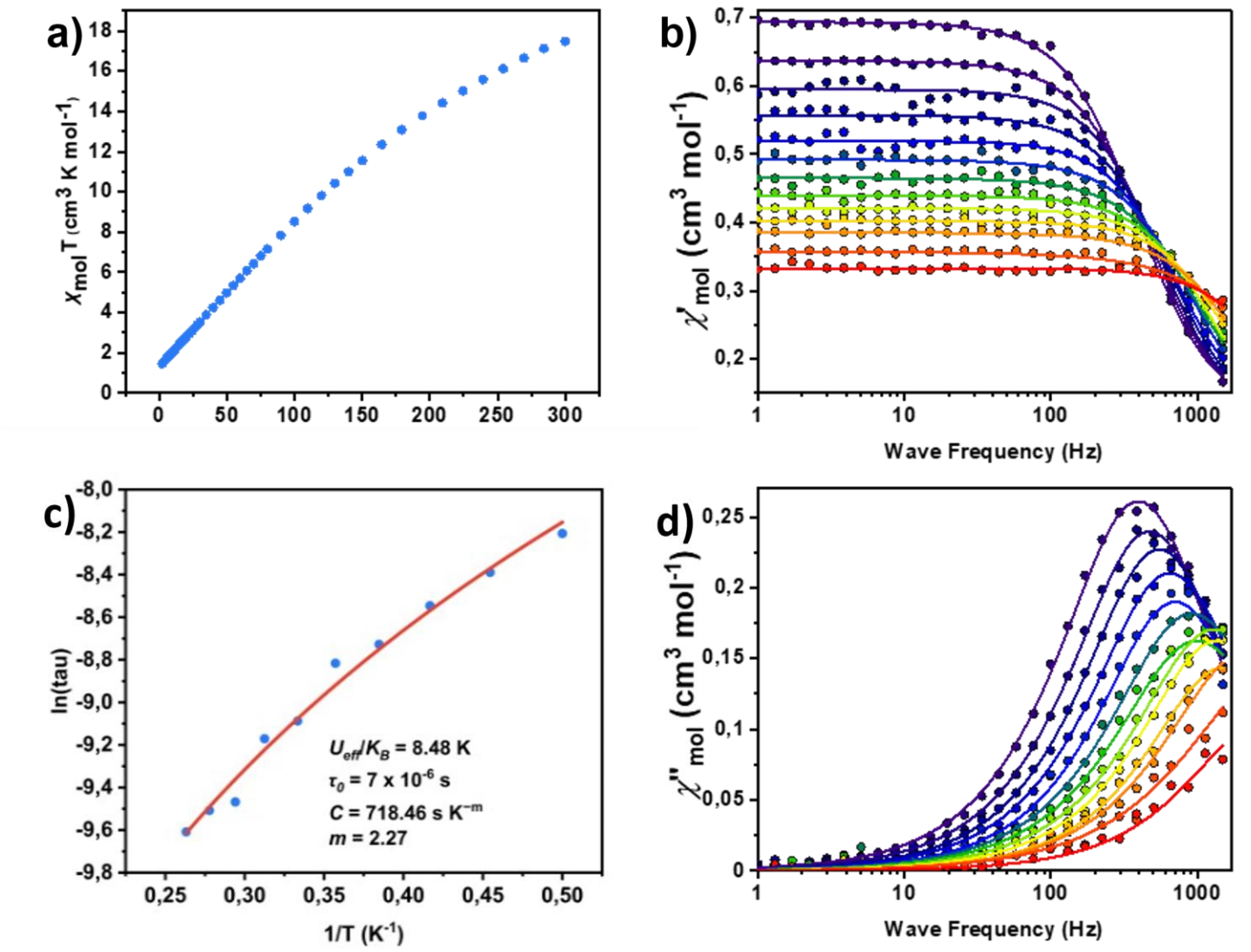

Figure 4: a) Eu_8Yb DC Fit: Temperature product of the molar susceptibility vs. temperature. c) Temperature dependence of the magnetization relaxation times (s), with the solid line representing the best fit using eqn (2) Red line: Raman contribution); (b,d) in-phase and out-of-

environment of discrete molecules.[59]

Photophysical Studies: The photophysical properties of the $[Eu_8Yb(BA)_{16}(OH)_{10}]Cl$ cluster have been studied at room temperature in CD_3OD solutions. Its UV-VIS-NIR absorption spectrum **(Figure. 5)** displays a broad band in the UV region with a maximum at 306 nm (ε = 28.4 x 10^4 $M^{-1}cm^{-1}$), attributed to transitions centered on the BA ligands, and a broad absorption band centered at 976 nm (ε = 12.95 $M^{-1}cm^{-1}$ in CD_3OD), which is attributed to the $^2F_{5/2} \leftarrow {}^2F_{7/2}$ transition of Yb^{III}.

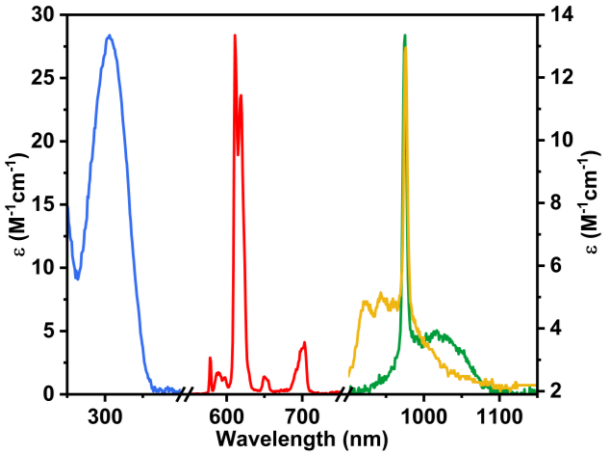

Figure 5. UV-Vis and NIR absorption spectra (blue (45 µM) and yellow (1 mM), respectively) and normalized emission spectra (λ_{exc} = 326 nm) in the visible (red: Eu, 45 µM, 399 nm Filter) and NIR (green: Yb, 45 µM, 800 nm Filter) domains for the Eu_8Yb cluster in CD_3OH.

broad emission band peaking at 974 nm corresponds to the $^2F_{5/2} \rightarrow {}^2F_{7/2}$ transition of Yb (Φ_{Yb} = 0.26% in CD_3OD). The corresponding luminescence lifetime of Yb in CD_3OD was 13.9 ± 0.1 µs at 974 nm. Lifetime and quantum yield values are similar to those reported for the Tb_1Yb_8 cluster with acac antennae.[30] According to the formalism of Werts and co-workers,[60] the radiative lifetime was estimated from the integral of the Yb absorption spectrum (SI. 2.2. Fig. 30.) to amount to 810 μs, which is in line with literature data on other Yb clusters.[30] With these values, the intrinsic quantum yield of Yb was calculated to be 1.7%, and the sensitization efficiency amounted to 16%, a result similar to the previously obtained value of 22% for unsubstituted acac-d7 ligands.[26]

Time-dependent luminescence decay profiles were also measured for the Eu^{III} emission (λ_{exc} = 326 nm) and fitted to bi-exponential curves with the corresponding lifetimes: τ_1 = 0.196 ± 0.001 ms (B_1 = 85 %), τ_2 = 1.265 ± 0.002 ms (B_2 = 15 %) measured at 578 nm, and τ_1 = 0.189 ± 0.001 ms (B_1 = 84 %), τ_2 = 1.256 ± 0.002 ms (B_2 = 16 %) at 612 nm, respectively. Both fits are in very good agreement and reflect the presence of the Eu^{III} ions in two distinct chemical environments: the peripheral site (τ_1), with a major contribution due to the direct photosensitization from the BA antennae, and the central site (τ_2), present in a smaller proportion but exhibiting a longer lifetime due to enhanced protection against non-radiative quenching by solvent molecules.[61] Overall, the Eu^{III} emission quantum yield was measured to be Φ_{Eu} = 0.13% in CD_3OD (λ_{exc} = 326 nm). The radiative lifetime of Eu was also estimated using the formalism of Werts et *al*[58] and was found to be 1.32 ms, in relatively good agreement with the value found for Yb, considering the uncertainties inherent in the method. Noteworthy, these values are significantly smaller than common values observed for Eu complexes with β-diketonate ligands.[62]

The relatively low quantum yield of Eu suggests either inefficient sensitization by the BA ligands or the occurrence of non-radiative quenching processes due to vibrations, concentration quenching,[63] or energy transfer to the Yb $^2F_{5/2}$ excited state. Quantification of the Eu → Yb energy transfer has been achieved by measuring the Eu luminescence lifetimes of the Eu_9 cluster. The corresponding values are τ_1 = 0.253 ± 0.001 ms (B_1 = 81.40%), τ_2 = 1.484 ± 0.002 ms (B_2 = 18.6%) for 578 nm emission peak and τ_1 = 0.256 ± 0.001 ms (B_1 = 79.5%), τ_2 =1.586 ± 0.002 ms (B_2 = 20.5%) at 612 nm. A decrease of approximately 24% in the τ_1 lifetime of Yb, as well as a 15% shortening of τ_2, were observed following the incorporation of Eu into the Yb_9 structure. This decrease of the averaged lifetime amounts to 18% and is ascribed to the energy transfer from Eu to Yb within Eu_8Yb. Consequently, the efficiency of this energy transfer was estimated to be 18%. In addition, a radiative lifetime of 1.65 ms was determined for this cluster, consistent with other values measured within this study.

In the same cluster, Stokes downshifted photo-luminescence of Yb in the NIR was also observed when exciting in the visible absorption band of Eu at 578 nm ($^5D_0 \rightarrow {}^7F_0$) in CD_3OD **(Figure 6a.)** The characteristic $^2F_{5/2} \rightarrow {}^2F_{7/2}$ Yb emission is observed, indicating that Yb sensitization occurs as a result of the of the energy transfer from the $^5D_0$ energy levels of Eu to the $^2F_{5/2}$ excited state of Yb. Based on this intermetallic communication, we thus focused on the reverse mechanism, namely the cooperative sensitization of Eu by Yb.

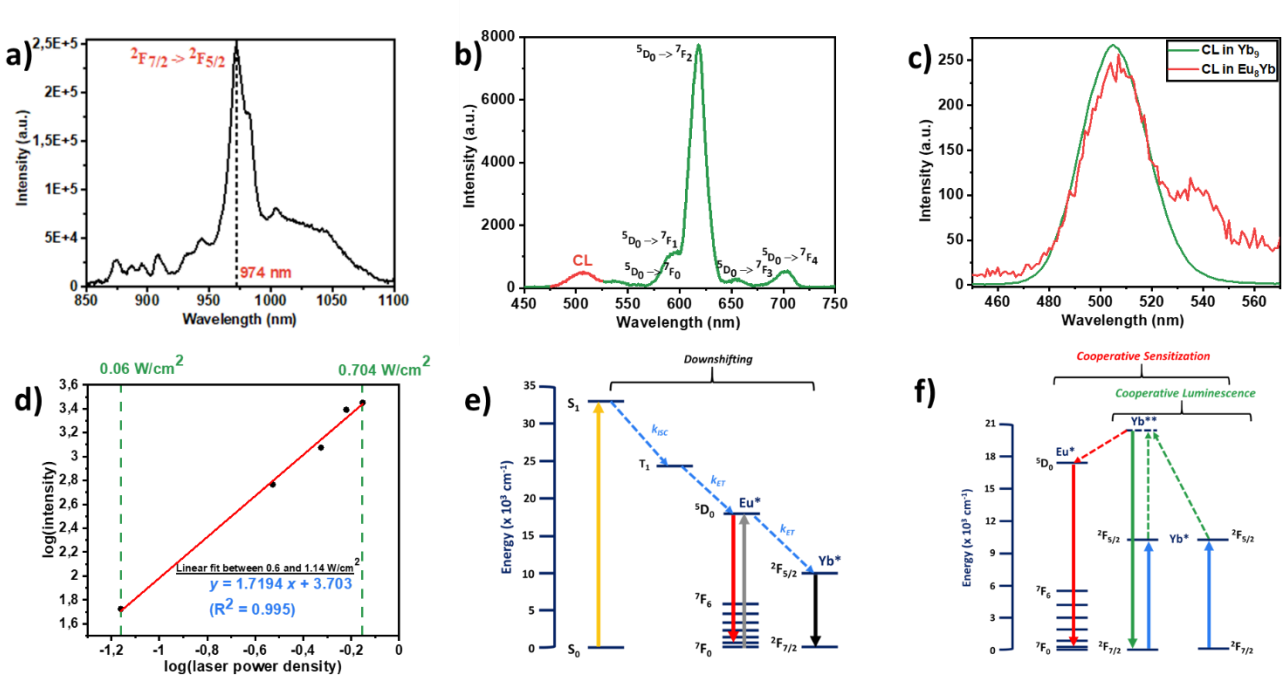

Figure 6. **a)** Downshifted PL emission of the Eu_8Yb complex ([c] = 0.5 mM, CD_3OD, λ_{exc} = 578 nm). **b)** UC emission of the Eu_8Yb complex ([c] = 45 µM, CD_3OD, λ_{exc} = 980 nm, P = 2.86 W cm^{-2}). **c)** Cooperative luminescence (CL) emission of the Yb_9 complex (Green, [c] = 2.04 mM, CD_3OD, λ_{exc} = 980 nm, P = 10.8 W cm^{-2}) vs CL emission of the Eu_8Yb complex (Red, [c] = 45 µM, CD_3OD, λ_{exc} = 980 nm, P = 10.8 W cm^{-2}), normalized according to the concentration of Yb^{3+} in the sample. **d)** UC intensity as a function of the incident pump power density in a log/log scale. **e)** Schematic representation of the absorption (yellow) and downshifting (black). f) Schematic representation of cooperative luminescence (green) and cooperative sensitization (red) process.

In ed
u of
te he
w re
at an

spectrum a strong emission in the visible region that had the typical spectral signature of the Eu emission with maxima at 612 nm and the five $^5D_0 \rightarrow {}^7F_J$ (J = 0 - 4) transitions (**Figure 6b**). Additionally, a small peak at 505 nm was also present which was assigned to the cooperative luminescence between two Yb centers (**Figure 6b**), as previously observed in homonuclear Yb_9 clusters.[26,30] Looking closely (**Figure 6c, red curve**), a weak and broad emission band was also noticed at 535-540 nm, which was attributed to the contribution of the $^5D_1 \rightarrow {}^7F_0$ emission, which is often observed in Eu β-diketonate complexes.[64] This observation is a strong argument to propose that the cooperative sensitization occurs from the doubly excited state of Yb to the $^5D_1$ level of Eu, with a subsequent population of the $^5D_0$ state.

The CL intensity from Eu_8Yb and Yb_9 was also compared (**Figure 6c**.) in order to gain insights into the influence of the Yb doping ratios on CL efficiency. Although a weak signal is measured from Eu_8Yb in comparison to Yb_9, this difference could mainly be ascribed to the variations in the Yb^{3+} concentrations (9 µM and 18.4 mM, respectively) of the two samples. In addition, it should be noted that, theoretically, CL can occur in clusters with a Yb:Eu 1:8 composition, owing to the statistical presence of clusters

in Yb), which could be explained by the reduction of concentration quenching.

To further confirm the upconversion luminescence mechanisms, the overall upconversion luminescent intensity (CS + CL) was recorded as a function of the incident pump power density, and the logarithmic representation presents a quasi-linear profile with slopes of 1.7 for CS at 612 nm and 1.6 for CL at 505 nm, respectively (Figure 6d and SI. 2.8. Fig. 31). The quadratic dependence provides evidence for the absorption of two photons by the Yb metal centers, in accordance with the upconversion mechanism.[48,65]

The proposed mechanism in a prototype complex, such as $Eu_{9-x}Yb_x$ (where x > 1), entails a major contribution of CS and a minor contribution of CL of Yb (**Figure 7**). As previously described, CS involves a first absorption of a photon by one Yb atom leading to a $[Eu_{9-x}Yb^*Yb_{x-1}]$ excited species, followed by the absorption of a second photon by a neighboring Yb ion, hence forming the $[Yb_2{}^{**}Eu_{9-x}Yb_{x-2}]$ intermediate which transfers its energy to $^5D_1$ and $^5D_0$ levels of Eu creating the $[Eu_{8-x}Eu^*Yb_x]$ excited states, which then decays to the ground state by emission of visible light. As for

Figure 7. Schematic representation of proposed cooperative photosensitization process UC mechanism.

CL, two photons absorption by two Yb ions in the same cluster results in a doubly Yb_2** excited state, which decays in the visible, showing a transition at 505 nm. As expected,

a $[Eu_9(BA)_{16}(OH)_{10}]Cl$ cluster without any Yb did not show any upconversion luminescence in the visible region when irradiated at 980 nm (SI. Fig. 2.8. 32).

Using established procedures,[25] we calculated the UC quantum yield (Φ_{UC}) of the $YbEu_8$ cluster in CD_3OD solution at room temperature, resulting in a value of 4.84×10^{-8} upon exciting at 980 nm (1.13 W cm^{-2}). This value is in line with previous data reported for UC quantum yields. It is 6 to 25 larger when compared to the best UC Er complexes ($1.95 \times 10^{-9} < \Phi_{UC} < 8 \times 10^{-9}$ at P= 21 W cm^{-2}),[48] and 3 times larger than the first hetero-polynuclear Yb/Tb UC complexes (1.4×10^{-8} at P= 10.3 W cm^{-2}). Nevertheless, this value is not as high as the quantum yields recently reported for Yb:Tb clusters,[26,30] which could be correlated to the increased propensity of Eu to be quenched by non-radiative deactivations. Another possible explanation for this reduced UC efficiency may be found in the lower spectral overlap of the CL emission of Yb** with the $^5D_1$ absorption band of Eu around 535 nm, compared to that of the $^5D_4$ absorption band of Tb at 485 nm. In conclusion, our findings highlight the role of supramolecular clusters in achieving efficient upconversion in solution by providing a scaffold capable of incorporating a unique lanthanide (Yb for CL) and/or donor/acceptor pairs (for CS) with appropriate Ln-Ln distances and a tunable statistical distribution. Additionally, we provide evidence of the potential to achieve cooperative sensitization (CS) upconversion and downshifting in a molecular cluster containing Eu and Yb.

Experimental Section:

Preparation of **$[Ln_nLn'_{9-n}(BA)_{16}(OH)_{10}]Cl$**.

Benzoylacetone (BA) (649 mg, 4 mmol, 4 eq.) and piperidine (396 ml, 4 mmol, 4 eq.) were dissolved in C_2H_5OH (60 ml). The mixture was heated while stirring at 75 °C for one hour. Meanwhile, $LnCl_3.6H_2O$ (x mmol, n/9 eq.) and $Ln'Cl_3.6H_2O$ (1-x mmol, (9-n)/9 eq.) were dissolved in 20 ml of H_2O and were added dropwise to the

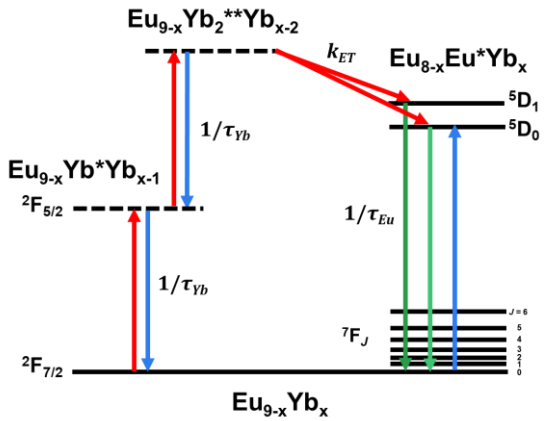

alcoholic solution, and the reaction mixture was stirred at 75 °C for three hours until obtaining a transparent solution. After three hours, the heating was turned off, and the solution cooled down to room temperature, filtered out, and left undisturbed to obtain crystals. After a week, we could harvest cubic-shaped crystals ideal for X-ray analysis. Details and characterization by XRD, ESI-TOF mass spectrometry, and elemental analysis are provided in the Supporting Information.

Conclusion

By doping Yb ions into Europium nonanuclear complexes, we were able to create a first-ever multifunctional heteronuclear $[Eu_8Yb(BA)_{16}(OH)_{10}]Cl$ complex that displays a highly efficient cooperative UC luminescence in solution based on the Yb/Eu donor/acceptor pair and a rare single-molecule magnet (SMM) behavior characterized by a slow relaxation of magnetization. The UC process is among the most efficient molecular or supramolecular UC probes reported to date[25,43,48] and can be observed in solution at concentrations as low as 100 nM. Furthermore, this marks a rare instance of direct cooperative sensitization (CS) upconversion within a molecular cluster that incorporates both Eu and Yb. By utilizing readily accessible β-diketonate ligands along with a diverse range of Ln donor-acceptor dyads and structures, we anticipate achieving even more efficient upconversion (UC) systems. In addition to the attractivity of UC systems for bio-analytical applications,[66] we believe that the development of UC luminescent Ln-SMMs is a promising field of research with many corners still unexplored. The incorporation of multiple functionalities into a single molecule can potentially enhance our understanding of SMM behavior, especially considering that SMMs are intended for implementation in next-generation nanocircuits for quantum computation.[67]

ASSOCIATED CONTENT

Supporting Information. Instrumentation, Crystallographic tables, figures of the packing of clusters, PXRD data, IR spectrum, SEM-EDX graphs, TG/DSC. Arrhenius plot data points. "This material is available free of charge via the Internet at http://pubs.acs.org."

AUTHOR INFORMATION

Corresponding Author

*E-Mail: mario.ruben@kit.edu
*E-Mail: l.charbonn@unistra.fr
*E-Mail: aline.nonat@unistra.fr

Funding Sources

European Union's Framework Programme for Research and Innovation, Horizon 2020, under the Marie Sklodowska-Curie Grant Agreement No. 847471 (QUSTEC).

Notes

The authors declare no competing financial interest.

ACKNOWLEDGMENT

Sai. P. K. Panguluri acknowledges late. Dr. Andreas Eichhöfer, Dr. Christopher E. Anson, Dr. Asato Mizuno, Dr. Olaf Fuhr, and Prof. Dieter Fenske for their assistance in PXRD and SC-XRD measurements.

REFERENCES

1. Nichia Corporation, Shimizu, Y., Sakano,; K., Noguchi. Y.; Moriguchi, T., Light Emitting Device With Blue Light Led And Phosphor Components, US7215074B2, May-08-2007.
2. Siemens Medical Solutions USA, Inc., Ghelmansarai, F. A., X-ray Scintillator Compositions For X-ray Imaging Applications, US6630675B2, October-07-2003.
3. J. Emsley, *Europium*, https://eic.rsc.org/elements/europium/2020007.article, accessed: 08/10/2019.
4. Intermetallics Co. Ltd [JP], Masato, S.; M., Tetsuhiko, M., Sintered Neodymium Magnet, EP2696355A1, February-05-2014.
5. Bünzli, J.-C. G., Lanthanide Luminescence for Biomedical Analyses and Imaging. *Chemical Reviews* **2010,** *110* (5), 2729-2755.
6. Eliseeva, S. V.; Bünzli, J.-C. G., Lanthanide luminescence for functional materials and bio-sciences. *Chemical Society Reviews* **2010,** *39* (1), 189-227.
7. Li, J.; Zhu, Y.; Xu, H.; Zheng, T.-F.; Liu, S.-J.; Wu, Y.; Chen, J.-L.; Chen, Y.-Q.; Wen, H.-R., A Benzothiadiazole-Based Eu3+ Metal–Organic Framework as the Turn-On Luminescent Sensor toward Al3+ and Ga3+ with Potential Bioimaging Application. *Inorganic Chemistry* **2022,** *61* (8), 3607-3615.
8. Liu, Y.; Lu, Y.; Yang, X.; Zheng, X.; Wen, S.; Wang, F.; Vidal, X.; Zhao, J.; Liu, D.; Zhou, Z.; Ma, C.; Zhou, J.; Piper, J. A.; Xi, P.; Jin, D., Amplified stimulated emission in upconversion nanoparticles for super-resolution nanoscopy. *Nature* **2017,** *543* (7644), 229-233.
9. Hamon, N.; Bridou, L.; Roux, M.; Maury, O.; Tripier, R.; Beyler, M., Design of Bifunctional Pyclen-Based Lanthanide Luminescent Bioprobes for Targeted Two-Photon Imaging. *The Journal of Organic Chemistry* **2023,** *88* (13), 8286-8299.
10. Park, Y. I.; Lee, K. T.; Suh, Y. D.; Hyeon, T., Upconverting nanoparticles: a versatile platform for wide-field two-photon microscopy and multi-modal in vivo imaging. *Chemical Society Reviews* **2015,** *44* (6), 1302-1317.
11. Chen, B.; Wang, F., Combating concentration quenching in upconversion nanoparticles. *Accounts of Chemical Research* **2019,** *53* (2), 358-367.
12. Bharmoria, P.; Bildirir, H.; Moth-Poulsen, K., Triplet–triplet annihilation based near infrared to visible molecular photon upconversion. *Chemical Society Reviews* **2020,** *49* (18), 6529-6554.
13. Richards, B. S.; Hudry, D.; Busko, D.; Turshatov, A.; Howard, I. A., Photon upconversion for photovoltaics and photocatalysis: a critical review: focus review. *Chemical Reviews* **2021,** *121* (15), 9165-9195.
14. Liu, S.; Yan, L.; Huang, J.; Zhang, Q.; Zhou, B., Controlling upconversion in emerging multilayer core–shell nanostructures: from fundamentals to frontier applications. *Chemical Society Reviews* **2022,** *51* (5), 1729-1765.
15. Yin, H.-J.; Xiao, Z.-G.; Feng, Y.; Yao, C.-J., Recent Progress in Photonic Upconversion Materials for Organic Lanthanide Complexes. *Materials* **2023,** *16* (16), 5642.
16. Nonat, A. M.; Charbonnière, L. J., Upconversion of light with molecular and supramolecular lanthanide complexes. *Coordination Chemistry Reviews* **2020,** *409*, 213192.
17. Bolvin, H.; Furstenberg, A.; Golesorkhi, B.; Nozary, H.; Taarit, I.; Piguet, C., Metal-based linear light upconversion implemented in molecular complexes: challenges and perspectives. *Accounts of Chemical Research* **2022,** *55* (3), 442-456.
18. a) Göppert-Mayer, M. (1931), Über Elementarakte mit zwei Quantensprüngen. Ann. Phys., 401: 273-294. b) N. Bloemberger, Phys. Rev. Lett. 2 (1959) 84-85 c) Auzel, F., Upconversion and Anti-Stokes Processes with f and d Ions in Solids. *Chemical Reviews* **2004,** *104* (1), 139-174.
19. Porter, J. F., Fluorescence Excitation by the Absorption of Two Consecutive Photons. *Physical Review Letters* **1961,** *7* (11), 414-415.
20. Auzel, F., Compteur quantique par transfert denergie de Yb3+ a Tm3+ dans un tungstate mixte et dans un verre germanate. *Comptes rendus hebdomadaires des seances de l academie des sciences serie b* **1966,** *263* (14), 819-&.
21. Auzel, F., Compteur quantique par transfert d'energie entre deux ions de terres rares dans un tungstate mixte et dans un verre. *C. R. Acad. Sci. Paris* **1966,** *262*, 1016-1019.
22. Salley, G. M.; Valiente, R.; Guedel, H. U., Luminescence upconversion mechanisms in Yb3+–Tb3+ systems. *Journal of Luminescence* **2001,** *94-95*, 305-309.
23. Livanova, L.; Saitkulov, I.; Stolov, A., Summation processes for quanta in CaF2 and SrF2 single crystals activated with Tb3+ and Yb3+ ions. *Sov. Phys. Solid State* **1969,** *11*, 750-754.
24. Souri, N.; Tian, P.; Platas-Iglesias, C.; Wong, K.-L.; Nonat, A.; Charbonnière, L. J., Upconverted photosensitization of Tb visible emission by NIR Yb excitation in discrete supramolecular heteropolynuclear complexes. *Journal of the American Chemical Society* **2017,** *139* (4), 1456-1459.
25. Nonat, A.; Bahamyirou, S.; Lecointre, A.; Przybilla, F.; Mely, Y.; Platas-Iglesias, C.; Camerel, F.; Jeannin, O.; Charbonnière, L. J., Molecular upconversion in water in heteropolynuclear supramolecular Tb/Yb assemblies. *Journal of the American Chemical Society* **2019,** *141* (4), 1568-1576.
26. Knighton, R. C.; Soro, L. K.; Lecointre, A.; Pilet, G.; Fateeva, A.; Pontille, L.; Francés-Soriano, L.; Hildebrandt, N.; Charbonniere, L. J., Upconversion in molecular hetero-nonanuclear lanthanide complexes in solution. *Chemical Communications* **2021,** *57* (1), 53-56.
27. Gao, C.; Zheng, P.; Liu, Q.; Han, S.; Li, D.; Luo, S.; Temple, H.; Xing, C.; Wang, J.; Wei, Y., Recent advances of upconversion nanomaterials in the biological field. *Nanomaterials* **2021,** *11* (10), 2474.
28. Magne, S.; Ouerdane, Y.; Druetta, M.; Goure, J.-P.; Ferdinand, P.; Monnom, G., Cooperative luminescence in an ytterbium-doped silica fibre. *Optics communications* **1994,** *111* (3-4), 310-316.
29. Chen, X.; Li, S.; Song, Z.; Du, W.; Wen, O.; Sawanobori, N., Study on strong cooperative upconversion luminescence of ytterbium-ytterbium clusters in oxyfluoride glass. *JOSA B* **2006,** *23* (12), 2581-2587.
30. Knighton, R. C.; Soro, L. K.; Francés-Soriano, L.; Rodríguez-Rodríguez, A.; Pilet, G.; Lenertz, M.; Platas-Iglesias, C.; Hildebrandt, N.; Charbonnière, L. J., Cooperative luminescence and cooperative sensitisation upconversion of lanthanide complexes in solution. *Angewandte Chemie International Edition* **2022,** *61* (4), e202113114.
31. a) Soro, L. K.; Knighton, R. C.; Avecilla, F.; Thor, W.; Przybilla, F.; Jeannin, O.; Esteban-Gomez, D.; Platas-Iglesias, C.; Charbonnière, L. J., Solution-State Cooperative Luminescence Upconversion in Molecular Ytterbium Dimers. *Advanced Optical Materials* **2023,** *11* (11), 2202307. b) Kushida, T.; Energy transfer and cooperative optical transitions in rare-earth doped inorganic materials. I. Transition probability calculation. *Journal of the Physical Society of Japan* **1973**, *34 (5)*, 1318-1326.
32. Haase, M.; Schäfer, H., Upconverting nanoparticles. *Angewandte Chemie International Edition* **2011,** *50* (26), 5808-5829.
33. Zheng, W.; Huang, P.; Tu, D.; Ma, E.; Zhu, H.; Chen, X., Lanthanide-doped upconversion nano-bioprobes: electronic structures, optical properties, and biodetection. *Chemical Society Reviews* **2015,** *44* (6), 1379-1415.
34. Gamelin, D. R.; Güdel, H. U., Design of luminescent inorganic materials: new photophysical processes studied by optical spectroscopy. *Accounts of chemical research* **2000,** *33* (4), 235-242.
35. Heer, S.; Kömpe, K.; Güdel, H. U.; Haase, M., Highly efficient multicolour upconversion emission in transparent colloids of lanthanide-doped NaYF4 nanocrystals. *Advanced Materials* **2004,** *16* (23-24), 2102-2105.
36. Suffren, Y.; Golesorkhi, B.; Zare, D.; Guénée, L.; Nozary, H.; Eliseeva, S. V.; Petoud, S.; Hauser, A.; Piguet, C., Taming

lanthanide-centered upconversion at the molecular level. *Inorganic Chemistry* **2016,** *55* (20), 9964-9972.
37. Charbonnière, L. J., Bringing upconversion down to the molecular scale. *Dalton Transactions* **2018,** *47* (26), 8566-8570.
38. Nonat, A.; Chan, C. F.; Liu, T.; Platas-Iglesias, C.; Liu, Z.; Wong, W.-T.; Wong, W.-K.; Wong, K.-L.; Charbonnière, L. J., Room temperature molecular up conversion in solution. *Nature Communications* **2016,** *7* (1), 11978.
39. Xiao, X.; Haushalter, J. P.; Faris, G. W., Upconversion from aqueous phase lanthanide chelates. *Optics letters* **2005,** *30* (13), 1674-1676.
40. Golesorkhi, B.; Nozary, H.; Guénée, L.; Fürstenberg, A.; Piguet, C., Room-Temperature Linear Light Upconversion in a Mononuclear Erbium Molecular Complex. *Angewandte Chemie* **2018,** *130* (46), 15392-15396.
41. Yin, H. J.; Feng, Y. S.; Liang, N.; Liu, X. M.; Liu, J. X.; Wang, K. Z.; Yao, C. J., Boosting Photo Upconversion in Electropolymerised Thin Film with Yb/Er Complexes. *Advanced Optical Materials* **2023,** *11* (6), 2202550.
42. Wang, J.; Jiang, Y.; Liu, J. Y.; Xu, H. B.; Zhang, Y. X.; Peng, X.; Kurmoo, M.; Ng, S. W.; Zeng, M. H., Discrete heteropolynuclear Yb/Er assemblies: switching on molecular upconversion under mild conditions. *Angewandte Chemie* **2021,** *133* (41), 22542-22549.
43. Aboshyan-Sorgho, L.; Besnard, C.; Pattison, P.; Kittilstved, K. R.; Aebischer, A.; Bünzli, J. C. G.; Hauser, A.; Piguet, C., Near-Infrared→ Visible Light Upconversion in a Molecular Trinuclear d–f–d Complex. *Angewandte Chemie International Edition* **2011,** *50* (18), 4108-4112.
44. Golesorkhi, B.; Taarit, I.; Bolvin, H.; Nozary, H.; Jiménez, J.-R.; Besnard, C.; Guénée, L.; Fürstenberg, A.; Piguet, C., Molecular light-upconversion: we have had a problem! When excited state absorption (ESA) overcomes energy transfer upconversion (ETU) in Cr (III)/Er (III) complexes. *Dalton Transactions* **2021,** *50* (23), 7955-7968.
45. Knighton, R. C.; Soro, L. K.; Thor, W.; Strub, J.-M.; Cianférani, S.; Mély, Y.; Lenertz, M.; Wong, K.-L.; Platas-Iglesias, C.; Przybilla, F.; Charbonnière, L. J., Upconversion in a d–f [RuYb3] Supramolecular Assembly. *Journal of the American Chemical Society* **2022,** *144* (29), 13356-13365.
46. Gálico, D. A.; Calado, C. M. S.; Murugesu, M., Lanthanide molecular cluster-aggregates as the next generation of optical materials. *Chemical Science* **2023,** *14* (22), 5827-5841.
47. Auzel, F.; Meichenin, D.; Pelle, F.; Goldner, P., Cooperative luminescence as a defining process for RE-ions clustering in glasses and crystals. *Optical Materials* **1994,** *4* (1), 35-41.
48. Golesorkhi, B.; Fürstenberg, A.; Nozary, H.; Piguet, C., Deciphering and quantifying linear light upconversion in molecular erbium complexes. *Chemical science* **2019,** *10* (28), 6876-6885.
49. a) D. A. Gálico, M. Murugesu, *Angew. Chem. Int. Ed.* **2022**, *61*, e202204839; *Angew. Chem.* **2022**, *134*, e202204839. b) Duan, X.-F.; Zhou, L.-P.; Li, H.-R.; Hu, S.-J.; Zheng, W.; Xu, X.; Zhang, R.; Chen, X.; Guo, X.-Q.; Sun, Q.-F., Excited-Multimer Mediated Supramolecular Upconversion on Multicomponent Lanthanide-Organic Assemblies. *Journal of the American Chemical Society* **2023,** *145* (42), 23121-23130. c) Xu, G.; Wang, Z.-M.; He, Z.; Lü, Z.; Liao, C.-S.; Yan, C.-H., Synthesis and structural characterization of nonanuclear lanthanide complexes. *Inorganic chemistry* **2002,** *41* (25), 6802-6807.
50. Baril-Robert, F.; Petit, S.; Pilet, G.; Chastanet, G.; Reber, C.; Luneau, D., Site-selective lanthanide doping in a nonanuclear yttrium (III) cluster revealed by crystal structures and luminescence spectra. *Inorganic chemistry* **2010,** *49* (23), 10970-10976.
51. Aguilà Avilés, D.; Roubeau, O.; Aromí Bedmar, G., Designed Polynuclear Lanthanide Complexes for Quantum Information Processing. *Dalton Transactions, 2021, vol. 50, p. 12045-12057* **2021**.
52. Marin, R.; Brunet, G.; Murugesu, M., Shining new light on multifunctional lanthanide single-molecule magnets. *Angewandte Chemie International Edition* **2021,** *60* (4), 1728-1746.
53. Brunet, G.; Marin, R.; Monk, M.-J.; Resch-Genger, U.; Gálico, D. A.; Sigoli, F. A.; Suturina, E. A.; Hemmer, E.; Murugesu, M., Exploring the dual functionality of an ytterbium complex for luminescence thermometry and slow magnetic relaxation. *Chemical Science* **2019,** *10* (28), 6799-6808.
54. Kumar, K. S.; Serrano, D.; Nonat, A. M.; Heinrich, B.; Karmazin, L.; Charbonnière, L. J.; Goldner, P.; Ruben, M., Optical spin-state polarization in a binuclear europium complex towards molecule-based coherent light-spin interfaces. *Nature Communications* **2021,** *12* (1), 2152.
55. Pointillart, F.; Cador, O.; Le Guennic, B.; Ouahab, L., Uncommon lanthanide ions in purely 4f Single Molecule Magnets. *Coordination Chemistry Reviews* **2017,** *346*, 150-175.
56. Kishi, Y.; Cornet, L.; Pointillart, F.; Riobé, F.; Lefeuvre, B.; Cador, O.; Le Guennic, B.; Maury, O.; Fujiwara, H.; Ouahab, L., Luminescence and Single-Molecule-Magnet Behaviour in Lanthanide Coordination Complexes Involving Benzothiazole-Based Tetrathiafulvalene Ligands. *European Journal of Inorganic Chemistry* **2018,** *2018* (3-4), 458-468.
57. Ruiz-Bilbao, E.; Pardo-Almanza, M.; Oyarzabal, I.; Artetxe, B.; Felices, L. S.; García, J. A.; Seco, J. M.; Colacio, E.; Lezama, L.; Gutiérrez-Zorrilla, J. M., Slow Magnetic Relaxation and Luminescent Properties of Mononuclear Lanthanide-Substituted Keggin-Type Polyoxotungstates with Compartmental Organic Ligands. *Inorganic Chemistry* **2022,** *61* (5), 2428-2443.
58. Errulat, Dylan, Riccardo Marin, Diogo A. Gálico, Katie LM Harriman, Amelie Pialat, Bulat Gabidullin, Fernando Iikawa et al. "A luminescent thermometer exhibiting slow relaxation of the magnetization: toward self-monitored building blocks for next-generation optomagnetic devices. *ACS Cent. Sci.* **2019** *(5, 7),* 1187–1198.

59. Gabarró-Riera, Guillem, Guillem Aromí, and E. Carolina Sañudo. "Magnetic molecules on surfaces: SMMs and beyond." *Coordination Chemistry Reviews* **2023,** *475,* 214858.
60. Werts, M. H.; Jukes, R. T.; Verhoeven, J. W., The emission spectrum and the radiative lifetime of Eu 3+ in luminescent lanthanide complexes. *Physical Chemistry Chemical Physics* **2002,** *4* (9), 1542-1548.
61. Beeby, A.; Clarkson, I. M.; Dickins, R. S.; Faulkner, S.; Parker, D.; Royle, L.; De Sousa, A. S.; Williams, J. G.; Woods, M., Non-radiative deactivation of the excited states of europium, terbium and ytterbium complexes by proximate energy-matched OH, NH and CH oscillators: an improved luminescence method for establishing solution hydration states. *Journal of the Chemical Society, Perkin Transactions 2* **1999,** (3), 493-504.
62. Shavaleev, N. M.; Eliseeva, S. V.; Scopelliti, R.; Bünzli, J.-C. G., Influence of symmetry on the luminescence and radiative lifetime of nine-coordinate europium complexes. *Inorganic chemistry* **2015,** *54* (18), 9166-9173.
63. Auzel, F.; A fundamental self-generated quenching center for lanthanide-doped high-purity solids. *Journal of Luminescence* **2002**, *100(1-4)*, 125-130.
64. Kadjane, P.; Charbonnière, L.; Camerel, F.; Lainé, P. P.; Ziessel, R., Improving visible light sensitization of luminescent europium complexes. *Journal of fluorescence* **2008,** *18*, 119-129.
65. Chen, G.; Qiu, H.; Prasad, P. N.; Chen, X., Upconversion nanoparticles: design, nanochemistry, and applications in theranostics. *Chemical reviews* **2014,** *114* (10), 5161-5214.
66. Wernsdorfer, W.; Ruben, M., Synthetic Hilbert Space Engineering of Molecular Qudits: Isotopologue Chemistry. *Advanced Materials* **2019,** *31* (26), 1806687.
67. Sun, L.; Wei, R.; Feng, J.; Zhang, H., Tailored lanthanide-doped upconversion nanoparticles and their promising bioapplication prospects. *Coordination Chemistry Reviews* **2018,** *364*, 10-32.

TOC Graphic:

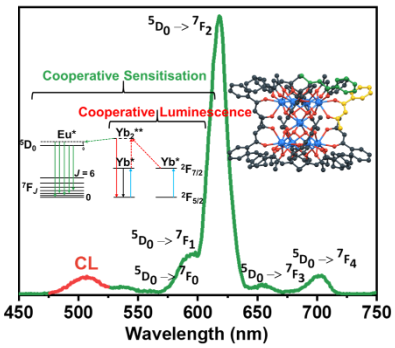
$^5D_0 \rightarrow {}^7F_2$
Cooperative Sensitisation
Cooperative Luminescence
Eu*
Yb_2**
Yb*
Yb* $^2F_{7/2}$
$^2F_{5/2}$
$^5D_0$
^7F_J
J = 6
0
$^5D_0 \rightarrow {}^7F_1$
CL
$^5D_0 \rightarrow {}^7F_0$
$^5D_0 \rightarrow {}^7F_3$
$^5D_0 \rightarrow {}^7F_4$
450
500
550
600
650
700
750
Wavelength (nm)